JACS
JOURNAL OF THE AMERICAN CHEMICAL SOCIETY
Article
pubs.acs.org/JACS

# Dramatically Enhanced Cleavage of the C−C Bond Using an Electrocatalytically Coupled Reaction

Qinggang He,[†,⊥] Badri Shyam,[‡,∥] Kateřina Macounová,[§] Petr Krtil,[§] David Ramaker,[‡] and Sanjeev Mukerjee*[,†]

[†]Department of Chemistry and Chemical Biology, Northeastern University, 360 Huntington Avenue, Boston, Massachusetts 02115, United States

[‡]Department of Chemistry, The George Washington University, 725 21st Street NW, Washington D.C. 20052, United States

[§]J. Heyrovsky Institute of Physical Chemistry, Academy of Sciences of the Czech Republic, Dolejškova 3, CZ-182 23 Prague 8, Czech Republic

Supporting Information

**ABSTRACT:** This paper describes a generalized approach for the selective electrocatalytic C−C bond splitting in aliphatic alcohols at low temperature in aqueous state, with ethanol as an example. We show that selective C−C bond cleavage, leading to carbon dioxide, is possible in high pH aqueous media at low overpotentials. This improved selectivity and activity is achieved using a solution-born co-catalyst based on Pb(IV) acetate, which controls the mode of the ethanol adsorption so as to facilitate direct activation of the C−C bond. The simultaneously formed *under-potentially deposited* (UPD) Pb and *surface lead hydroxide* change the functionality of the catalyst surface for efficient promotion of CO oxidation. The resulting catalyst retains an unprecedented ability to sustain the full oxidation reaction pathway on an extended time scale of hours as opposed to minutes without addition of Pb(IV) acetate.

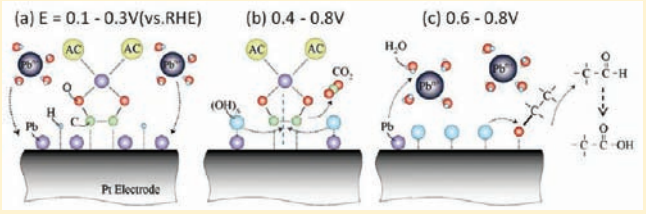


## 1. INTRODUCTION

The controlled electrocatalytic cleavage of the C−C bond in organic molecules, particularly in aliphatic alcohols, remains one of the most challenging problems in electrochemistry. Aside from a fundamental interest in directing a multielectron transfer to selectively cleave or form C−C bonds,[1] the reaction is also of great practical significance in the development of fuel cell-based electric energy generators.[2,3] This implementation enabling higher alcohol oxidation can significantly improve the energy density of these low-temperature fuel cells. The inertness of the C−C bonds in electrocatalytic alcohol oxidation is counterintuitive, since the C−C bonds are relatively weak and can be, in the case of hydrocarbons, cracked either thermally or catalytically.[4] Taking ethanol as an example, a cleavage of the C−C bond in the oxidation process leading eventually to $CO_2$ formation (12 electrons) is severely disfavored kinetically, especially in acid media.[5] The electrocatalytic oxidation of aliphatic alcohols proceeds readily on Pt-based metal surfaces but usually yields just 2−4 electrons per alcohol molecule, and depending on both the electrode material and the pH, rarely involves C−C bond splitting.[6−8] The resulting products are mostly the undesired aldehydes or corresponding acids at low pH. In contrast, in alkaline media, more complete oxidation occurs, mainly due to higher sensitivity to structural and morphological moieties such as the relative population of crystallite planes.[9,10] Ethanol oxidation, selective to $CO_2$, has been reported for Pt polarized to potentials in the oxygen evolution region in alkaline media.[11] The oxidation process is, however, far from controlled at these conditions.

Regardless of the media, Pt-based materials represent the benchmark catalysts for ethanol oxidation. There have been several strategies devised for enhancing the activity and selectivity of electrocatalytic ethanol oxidation,[12−15] some based on incorporation of adatoms to the surface. The enhancement has been attributed to steric hindrance of the surface, or electronic ligand and/or bifunctional effects when the adatoms are directly involved in the catalytic process.[16] The activity of purely metal-based catalytic systems is reported to be surpassed by multifunctional catalysts featuring metal oxide-based oxidation promoters like, for example, MgO,[17] $CeO_2$,[18] $ZrO_2$,[19] or $SnO_x$.[7,20] Despite the apparent improvement of the activity in the ethanol oxidation, the resulting selectivity of the oxidation process toward the desired 12 electron process still significantly lags behind expectations, with a gradual deactivation of the catalyst surface in the course of minutes. The rationalization for the C−C bond inactivity in ethanol oxidation arises because the ethanol molecule primarily adsorbs on the metal surface via the oxygen on the $C_1$ carbon. The first electron removed from the ethanol molecule facilitates formation of the energetically more stable aldehyde, which

**Received:** February 28, 2012
**Published:** April 19, 2012

   dx.doi.org/10.1021/ja301992h | *J. Am. Chem. Soc.* 2012, 134, 8655−8661

then easily desorbs from the surface preventing further charge transfer that could attack the ethanol C−C bond.[21,22] It may be envisaged that controlling the approach, and hence the adsorption mode of ethanol, toward the substrate could be instrumental in steering the selectivity of the oxidation process toward the C−C bond splitting essential for the complete oxidation route.

The present paper shows for the first time the successful application of this concept, utilizing a solution-based co-catalyst to direct the ethanol adsorption, while modifying the catalyst surface chemistry to oxidize selectively the C−C bond in ethanol. Differential electrochemical mass spectrometry (DEMS) and in situ X-ray absorption near-edge spectroscopy (XANES) data are used to show and rationalize the behavior of the Pb(IV) acetate under reaction conditions, thus, modifying the behavior of the Pt/C nanoparticulate catalyst to retain an unprecedented activity and selectivity toward C−C bond breaking on the time scale of hours.

## 2. EXPERIMENTAL METHODS

**2.1. Electrochemical Characterization.** The deposited Pb electrode was prepared as follows: (1) A Pt/C (E-TEK, 30%) electrode was cycled in 0.25 M KOH + 1 mM $Pb(Ac)_4$ between potential limits of 1.1 and 0.06 V ending at 0.06 V. (2) The electrode was taken out and transferred into 0.25 M KOH + 1 M ethanol after washing. (3) A cyclic voltammogram between potential limits of 0.2 and 1.1 V was obtained followed by a 1 h chronoamperometry (CA) test at 0.55 V. The "component" Pb samples, $Pt_4Pb$/C and $PtRuPb_{0.3}$/C, were synthesized from a Pt/C (30%, E-TEK) and PtRu/C (40%, E-TEK) catalyst and the Pb added by Li's method.[23] Detailed information about the chemicals and procedures for the electrochemical characterization can be found in the Supporting Information.

**2.2. X-ray Absorption Spectroscopy.** All experiments were conducted at room temperature in an *in situ* electrochemical XAS cell based on a previously reported design.[24] The cells consisted of a 30 wt % Pt/VXC72 (E-TEK) working electrode (WE), a Grafoil counter electrode (CE), and a reversible hydrogen reference electrode (RHE). Grafoil was chosen as a CE to eliminate any interference at the Pt $L_{3,2}$ edges and decrease X-ray beam attenuation. In all cases, Au wire (99.999%, Alfa-Aesar) was utilized as a current collector and mechanically pressed against the back side of the electrode in a fashion which did not expose the gold to the X-ray beam. The platinum working electrodes were activated by potential cycling (0.05−1.2 V vs RHE at 10 mV $s^{-1}$) in clean 0.25 M KOH. Following the activation step, the clean electrolyte was removed from the cell by syringe and replaced with 0.25 M KOH + *x*M $PbAc_4$. XAS data were collected from −250 to ca. 1000 eV above the Pt $L_3$ edge with the WE fixed at various static potentials along the anodic sweep of the cyclic voltammetric (CV) measurement. Between extended X-ray absorption fine structure (EXAFS) scans, the potential was cycled around completely to "clean" the electrode surface. A full set of EXAFS scans was also obtained in clean 0.25 M KOH to provide clean reference scans and as $H_2O$ activation standards. The measurements were made at beamline X11-A (National Synchrotron Light Source, Brookhaven National Laboratory, Upton, NY) with the Si(111) monochromator detuned by 40% in order to reject the higher harmonics from the beam. Data were collected in transmission mode using gas ionization detectors ($I_0$, $I_1$, or $I_2$) with a nominal nitrogen/argon gas mixture to allow ∼10% photon absorption in $I_0$ and 70% in $I_1$. The sample was placed between the $I_0$ and $I_1$ detectors, while a Pt reference foil (4 $\mu$m, Alfa Aesar) was positioned between $I_1$ and $I_2$.

The IFEFFIT suite[25] (version 1.2.8, IFEFFIT Copyright 2005, Matthew Newville, University of Chicago, http://cars9.uchicago.edu/ifeffit/) was utilized for background subtraction (AUTOBK).[26] The $\Delta\mu$ analysis technique has been described in great detail elsewhere.[27−29] Briefly, XAS reference scans were carefully calibrated to the edge energy (11564 eV, Pt $L_3$) and aligned to one standard reference scan. Any edge shift corrections applied to the reference foils were also applied to their respective sample scans. A post-edge normalization procedure was then applied to the aligned scans as described previously.[30] Difference spectra were obtained using the equation

$$\Delta\mu = \mu(\mathrm{V}) - \mu(0.54\ \mathrm{V}) \quad (1)$$

where $\mu$(V) is the sample at various potentials and $\mu$(0.54) is the reference signal at 0.54 V, which is considered the cleanest region of Pt, that is, relatively free of any adsorbed H, OH, or $O_x$ species. The $\Delta\mu$ spectra are then compared to theoretical curves ($\Delta\mu_t$) constructed using the FEFF8.0 code[31] as described elsewhere.[32] This was accomplished using the relationship

$$\Delta\mu_t = \mu(\mathrm{Pt_6X}) - \mu(\mathrm{Pt_6}) \quad (2)$$

where X is H or O in a specified binding site with respect to the absorbing Pt atom and $Pt_6$ is a 6-Pt cluster with a Pt−Pt bond distance of 2.77 Å as described by Janin et al.[33] It should be noted that theoretical $\Delta\mu$ curves are generally shifted by 1−5 eV and scaled by a multiplication factor for optimal comparison with experimental data.

**2.3. DEMS.** The analysis of the ethanol oxidation products generated in potentiostatic oxidation of ethanol was done by means of DEMS in a single compartment three electrode flow through cell made of PTFE. The DEMS apparatus consisted of a Prisma QMS200 quadrupole mass spectrometer (Balzers) connected to a TSU071E turbomolecular drag pumping station (Balzers). The DEMS data were recorded simultaneously with the current corresponding to the potentiostatic ethanol oxidation both in the presence and in absence of the co-catalyst. The treatment of the raw data along with information on construction of the calibration curves is given in the Supporting Information. The DEMS and XAS measurements were not carried out simultaneously owing to the vastly differing experimental requirements and constraints of the two techniques.

## 3. RESULTS AND DISCUSSION

The ethanol oxidation on Pt nanoparticulate (3−4 nm) electrocatalysts is relatively sluggish and proceeds without apparent C−C bond splitting in the potential window between 0.55 and 0.9 V (vs RHE, pH 14). The addition of Pb(IV) acetate (mM conc., in electrolyte soln.) significantly facilitates the oxidation process as indicated by a negative shift in the onset potential of ca. 150 mV, and a 3-fold increase of the current density, confirming the significant improvement of the ethanol oxidation kinetics (Figure 1). Although variation of

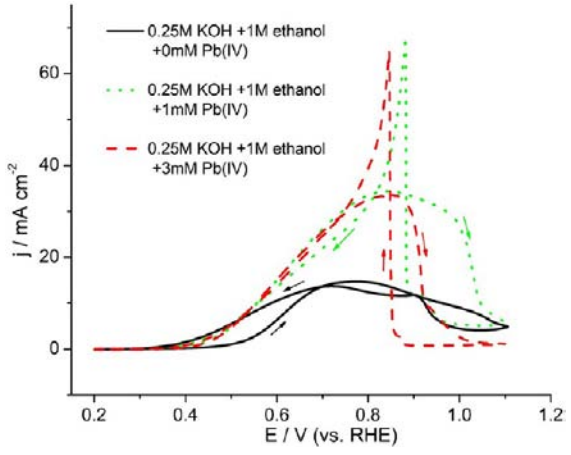


**Figure 1.** Cyclic voltammograms of Pt/C (E-TEK, 30%), in 0.25 M KOH + 1 M ethanol with 0, 1, and 3 mM Pb(IV); Pt loading, 15 $\mu$g/cm$^2$; scan rate, 10 mV/s. The CVs are normalized based on the geometric area of the glassy carbon electrode.


dx.doi.org/10.1021/ja301992h | J. Am. Chem. Soc. 2012, 134, 8655−8661

Pb(IV) acetate concentration does not necessarily alter the overall ethanol oxidation rate, it alters the potential window available for oxidation due to a change of the surface chemistry (Figure 1). The effect of the Pb(IV) acetate on the surface chemistry is also reflected in the cathodic response, which indicates more efficient removal of the oxidation reaction products from the electrode surface than when the Pb co-catalyst is absent. The remarkable stability of the Pt catalyst in the presence of Pb(IV) acetate (in soln.) is also evident from the chronoamperometric experiments, wherein the presence of the co-catalyst leads to a retention of ca. 56% of the initial current after 1 h (Figure 2). Similar yet slightly inferior results

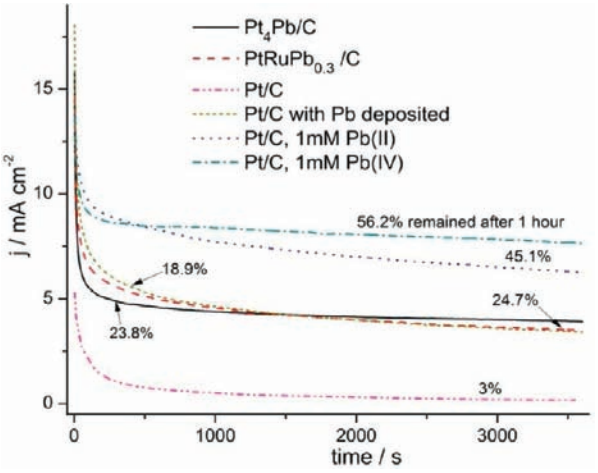


**Figure 2.** Chronoamperometry data for Pt/C (E-TEK, 30%), Pt4Pb/C (30%), PtRuPb0.3/C (40%), and Pt/C (E-TEK, 30%) with Pb deposited in 0.25 M KOH + 1 M ethanol. Also shown is data for Pt/C (E-TEK, 30%) in the same 0.25 M KOH + 1 M ethanol solution but with 1 mM Pb(IV) acetate or 1 mM Pb(II) acetate added; Pt loading, 15 $\mu$g/cm$^2$.

are found with Pb(II) acetate. The ethanol oxidation on Pt modified by lead deposition (UPD) shows a much steeper drop in activity compared with the case where Pb acetate is present in the electrolyte solution, although the behavior is superior to pure Pt, which retains just 3% of the original activity after 1 h. The trends summarized in Figure 3 reflect the complex nature of the Pb(IV) acetate functionality in the catalytic process.

The chronoamperometric response shown in Figure 3 shows the clear advantage of Pb(IV) as an electrolyte additive in a homogeneous–heterogeneous co-catalyst role for not only enhancing the activity but also ensuring sustained current densities as indicated in the steady-state current versus potential plot (inset, Figure 3). The presence of Pb(IV) in solution is expected to form a dynamic equilibrium with UPD adatoms of Pb formed at the Pt surface; the simultaneous presence of Pb in solution enables an apparent bifunctional mechanism to be combined with an apparent solution-based process responsible for the extraordinary activity retention. These chronoamperometric responses also indicate interesting differences in the capacitive currents, in the presence of co-catalyst wherein PtRu shows much higher capacitive charging currents as compared to response from Pt. This is particularly manifest at lower potentials (Figure 3).

Figure 4 gives a proposed ethanol oxidation reaction (EOR) mechanism based on DFT calculations,[34] and FTIR data.[5,35,36] Lai et al.[36] have shown that the orientation of the ethanol adsorption dictates which path the oxidation follows. Most

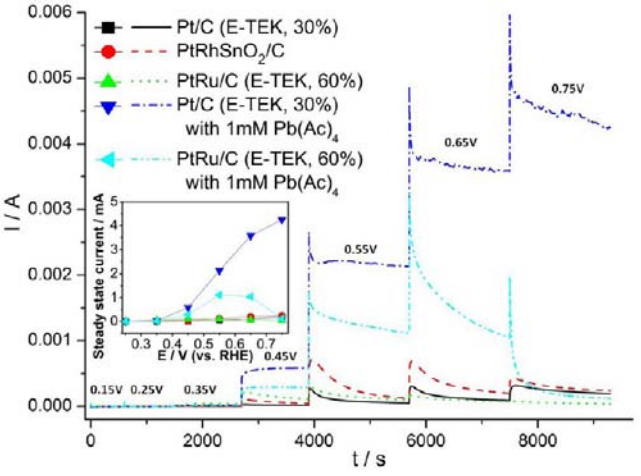


**Figure 3.** Chronoamperometry data, at the indicated potentials (vs RHE) in 0.25 M KOH + 1 M ethanol; Pt loading, 15 $\mu$g/cm$^2$; room temperature. Inset: Plots of steady current from the same data.

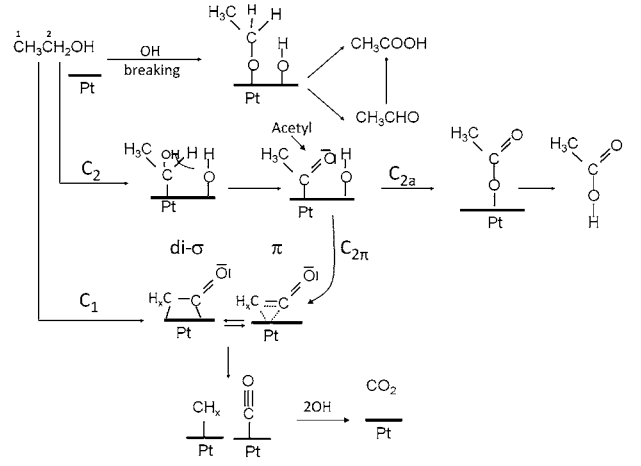


**Figure 4.** Proposed mechanism for EtOH oxidation on Pt.

often, particularly on the Pt(111) planes, only 4 electrons are evolved to produce acetic acid ($CH_3CH_2OH + H_2O \rightarrow CH_3COOH + 4e^- + 4H^+$) (the OH path). Bimetallics such as PtSn and PtMo normally give higher currents with ethanol than pure Pt, but unfortunately, the selectivity is shifted predominantly toward acetic acid product (path $C_{2a}$), that is, less efficient use of the ethanol fuel.[5,37] To accomplish the complete oxidation of ethanol, the initial adsorption of C atoms has to follow a $C_1$ or $C_2$ pathway; both of which have the potential of forming the crucial $\pi$ bonded species on Pt enabling effective cleavage of the C–C bond. These are denoted as the $C_1$ and $C_{2\pi}$ pathways. These steps are, however, highly energetically disfavored as shown by recent DFT calculations.[34] As we will show below, addition of a Pb(IV) co-catalyst enables the selective formation of such $\pi$-bonded ethylene species.

To rationalize the electrochemical enhancement and mechanism (e.g., the $C_1$ path or the $C_{2\pi}$ in Figure 4) of complete ethanol oxidation with the aid of a co-catalyst, unambiguous detection and quantification of $CO_2$ is essential. The lack of chemical sensitivity of many electrochemical techniques and the interfering effect of residual carbonates were avoided in this work by labeling the substrate ethanol with $^{13}C$ in the $C_2$ position. The $^{13}CO_2$ ($m/z$ = 45) detected in the reaction mixture, at levels well exceeding the natural abundance


dx.doi.org/10.1021/ja301992h | J. Am. Chem. Soc. 2012, 134, 8655–8661

of $^{13}C$, during chronoamperometric oxidation experiments mass spectroscopically proves conclusively the C−C bond splitting. The selectivity of the anodic process toward C−C bond cleavage significantly increases in the presence of Pb co-catalyst (Figure 5).

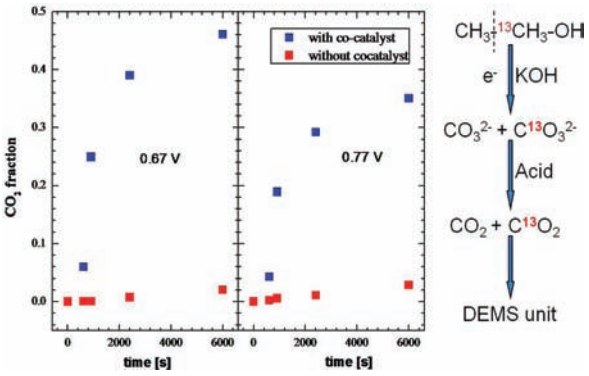


**Figure 5.** Charge fractions corresponding to $CO_2$ formation in catalytic oxidation of ethanol (0.01 M) in 0.25 M KOH on nanocrystalline Pt in presence and absence of lead co-catalyst. Data were extracted from potentiostatic oxidation experiments with $CH_3{}^{13}CH_2OH$.

The $CO_2$ selectivity increases with time (Figure 5) and reaches ca. 50% of its initial activity value after approximately 1 h (Figure 2). This trend confirms the anticipated competition between the $C_{2\pi}$ and $C_1$ kinetic oxidation mechanisms (Figure 4) at the surface. While the $C_{2\pi}$ mechanism deactivates rather quickly, the co-catalyst assisted $C_1$ mechanism apparently is deactivation resistant. The selectivity toward $CO_2$ production follows the same potential dependence as the observed catalytic current. Detailed accounts of the mass spectrometric experiments are given in the Supporting Information (Figure S4 in Supporting Information).

The promoting effect of Pb(IV) on electrooxidation of methanol and ethanol can be distinguished from the steady-state current density values obtained at different potentials shown in Figure 6. It can be clearly seen that the electrooxidation of ethanol can be enhanced much more

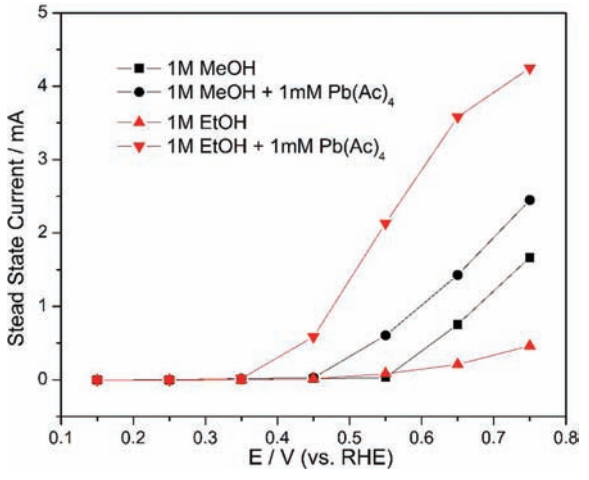


**Figure 6.** Chronoamperometry test comparison of Pt/C (E-TEK, 30%), as a function of potential in 0.25 M KOH + 1 M ethanol/methanol with 0 and 1 mM Pb(IV); Pt loading, 15 $\mu g/cm^2$.

dramatically than that of methanol with the assistance of Pb(IV) co-catalyst. It indicates that the C−C bond in ethanol can be efficiently broken by using Pb(IV) salts.

As can be seen from Figure 7, lead(IV) acetate from the electrolyte deposits at the Pt surface via underpotential

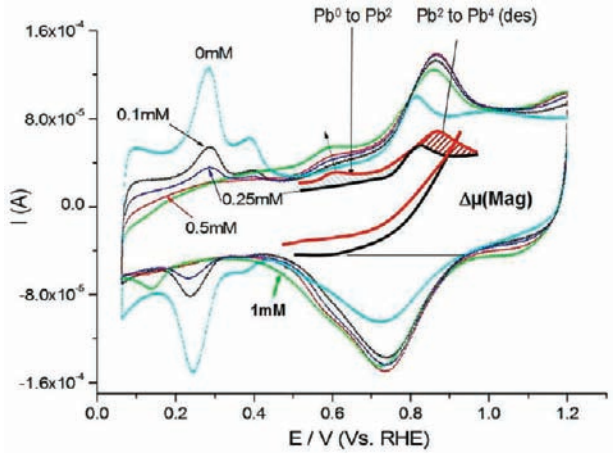


**Figure 7.** Cyclic voltammograms for Pt/C (E-TEK, 30%), in 0.25 M KOH with $x$ mM Pb(IV) acetate as indicated; Pt loading, 15 $\mu g/cm^2$. Inset shows $\Delta\mu$ magnitudes reflecting OH/Pt coverage with (red) and wiyhout Pb (black) and also highlights the difference between the 0.0 and 0.25 mM CV curves (see also Supporting Information Figures S2 and S3).

deposition at potentials negative of 0.4 V. The coverage of Pb adatoms on the Pt surface grows as the concentration of Pb(IV) ions increases and becomes saturated at the concentration about 0.5 mM. The UPD lead layer suppresses the hydrogen adsorption (Figure 7) and oxidizes to stable Pb $(OH)_2$ at 0.6 V, which is removed from the surface as $PbO_2$ when potential moves further positively.[38] The formation of the UPD lead layer and its subsequent oxidation can be correspondingly tracked in the increase of intensity of *in situ* XANES derived $\Delta\mu$ data (which is referred to as '$\Delta\mu$-XANES' and tracks OH adsorption) shown in Figure S3 (Supporting Information) and Figure 7, and also shows up as sudden jumps in the current response following the potentiostatic oxidation of ethanol in the presence of Pb(IV) acetate at potentials positive to 0.6 V (Figure 3); these jumps reflect the sudden increase of capacitance resulting from hydroxide growth. The bifunctional effect of the UPD lead layer is confined to the region of the lead hydroxide stability, which is broader on pure Pt than on the more complex Pt−Ru catalysts (Figure 3).

The bifunctional mechanism is instrumental in explaining the increased activity of anode catalysts based on the combination of Pt with oxophilic metals such as Ru, Sn, or Mo or in this case Pb in, for example, methanol or formic acid oxidation. The oxophilic metal provides the OH species needed to oxidize adsorbed CO. There is no indication of particular specific attack to the C−C bond by the bifunctional catalysts; in fact, the data shown in Figure 2 suggest rather inefficient C−C bond splitting, if the effect of the lead in the catalytic process is restricted to UPD deposited adatoms. The results reveal a pronounced deactivation of Pt−Pb alloy or Pt−Pb UPD catalysts with time (Figure 2). The key aspect of the reported efficient C−C bond splitting is, therefore, the presence of Pb(IV) acetate in solution and its interaction with the C−C bond of ethanol preceding the electron transfer. This


dx.doi.org/10.1021/ja301992h | J. Am. Chem. Soc. 2012, 134, 8655−8661

interaction is not of a purely redox nature, as shown by the almost identical response for divalent as well as tetravalent lead acetate.

The preferred adsorption mode of the ethanol at the electrode normally involves binding through the oxygen (i.e., the OH path); this is facilitated by the electrostatics of the surface at anodic potentials.[39] In contrast, the interaction between ethanol and Pt is tracked in the $\Delta\mu$-XANES data plotted in Figure 8. The data acquired on Pt in the absence of

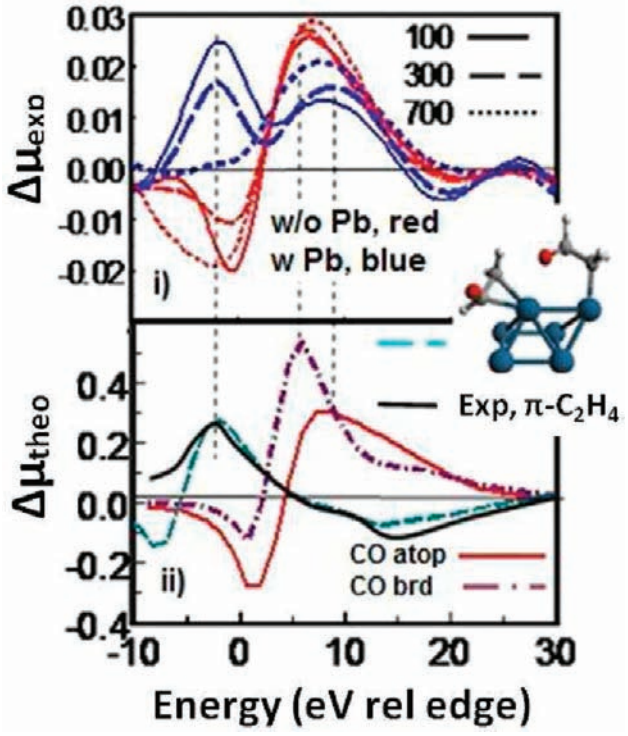


**Figure 8.** (i) Plot of $\Delta\mu = \mu(V) - \mu(0.5\ V, cl)$ for Pt with (1 mM $PbAc_4$) and without $PbAc_4$ in 0.2 M ethanol + 0.25 M KOH at the indicated potentials, mV. (ii) Theoretically calculated $\Delta\mu = \mu(Ad/Pt_6) - M(Pt_6)$ using FEFF8 for the indicated adsorbates as illustrated; CO/Pt in either an atop or bridged site, and for ethanol in a $\pi$-bonded geometry (that for the $\sigma$-bonded is nearly identical so it is not shown). Also shown is experimental $\Delta\mu$ data for $\pi$-bonded ethylene.

Pb(IV) acetate (red curves in Figure 8(i)) can be rationalized in terms of the accumulation of bicarbonate and chemisorbed CO in 'bridged' and 'atop' positions at the electrode surface. The bicarbonate is present at the surface only at potentials close to 0.1 V and yields chemisorbed CO at more positive potentials. The chemisorbed CO moves more to the atop position with decreasing surface coverage at more positive potential.[40,41] This tendency for CO adsorption is essentially in accordance with previous studies carried out by means of infrared spectroscopy by Lai et al.[36] When the lead acetate-based co-catalyst is present (blue curves in Figure 8(i)), the observed $\Delta\mu$-XANES data indicates accumulation of atop CO on the surface at potentials positive to 0.5 V. The $\Delta\mu$ features dominating at potentials negative to 0.3 V, that is, at potentials negative to the ethanol oxidation window, centered at −5 eV cannot be attributed to species present on a pure Pt electrode surface and therefore suggest an adsorbed ethanol moiety. The quantum chemistry-based adsorption models best fitting the experimental $\Delta\mu$-XANES data are depicted in Figure 8(ii) and also agree with previously reported experimental $\Delta\mu$-XANES data for ethylene on Pt(111).[42] Both proposed adsorption modes assume an attachment of the ethanol to the surface via the C1 carbon, either $\sigma$-bonded or ethylene-like $\pi$-bonded. Both modes of adsorption allow for direct activation of the C−C bond, but the C1 adsorption has to be directed somehow by interaction with the co-catalyst to overcome the electrostatically preferred adsorption via the oxygen end of the molecule.

Similar effects with cations directing the adsorption at the electrodes were described recently.[43] These interactions have been reported to occur between hydrated cations in the outer Helmholtz plane (OHP) and specifically adsorbed OH in the inner Helmholtz plane (IHP) as illustrated in Figure 9. Note

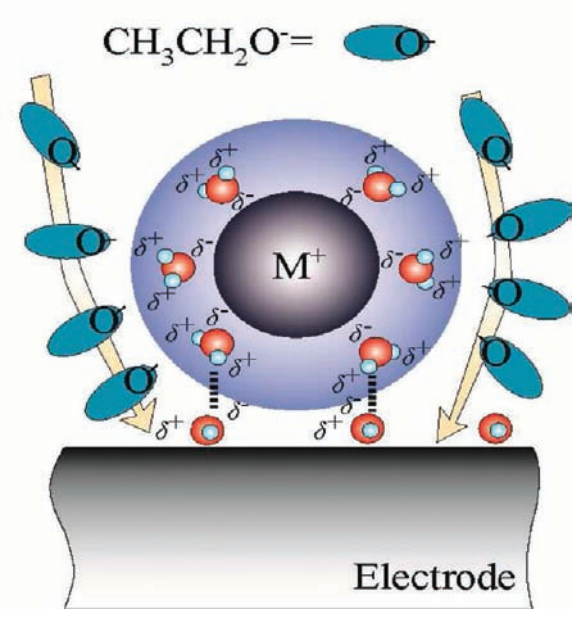


**Figure 9.** Possible mechanism for how noncovalent interactions with the hydrated Pb cations may provide a preferred orientation of acetaldehyde anion with the $CH_3$ end pointing toward the surface as it approaches.

that the electrostatic interaction between the waters hydrating the Pb cation and the approaching ethanol causes the carbon end of the molecule to preferably approach the electrode surface. An alternative explanation can be derived from the known fact that Pb complexes like $Pb(Ac)_4$ and $Pb(benzoate)_4$ are able to facilitate C−C and C=O bond dissociation in nonaqueous media,[44] forming chelates with alcohol molecules.

A similar effect may be operating also in this case. The effect of the co-catalyst activity is summarized in the scheme shown in Figure 10. In panel a, it shows that a possible Pb−acetate−chelate complex and Pb adatoms can be formed simultaneously due to the presence of $Pb(^{n+})$ ions in the solution when the potential is lower than 0.3 V. This is an important role of the co-catalyst namely to isolate the ethanol from the Pt substrate while modifying the Pt surface. This cannot be realized by the bifunctional catalysts (e.g., PtRu and PtSn) or UPD adatom modified Pt catalysts. In panel b, ethanol molecules near the surface, through their energetically favorable binding with the Pb(IV), are weakly bonded to the surface through the carbon as opposed to the usual binding through the electron rich oxygen atom (OH pathway). The adsorbed moiety then reacts with the surface OH species on Pb adatoms to directly cleave the C−C


dx.doi.org/10.1021/ja301992h | J. Am. Chem. Soc. 2012, 134, 8655−8661

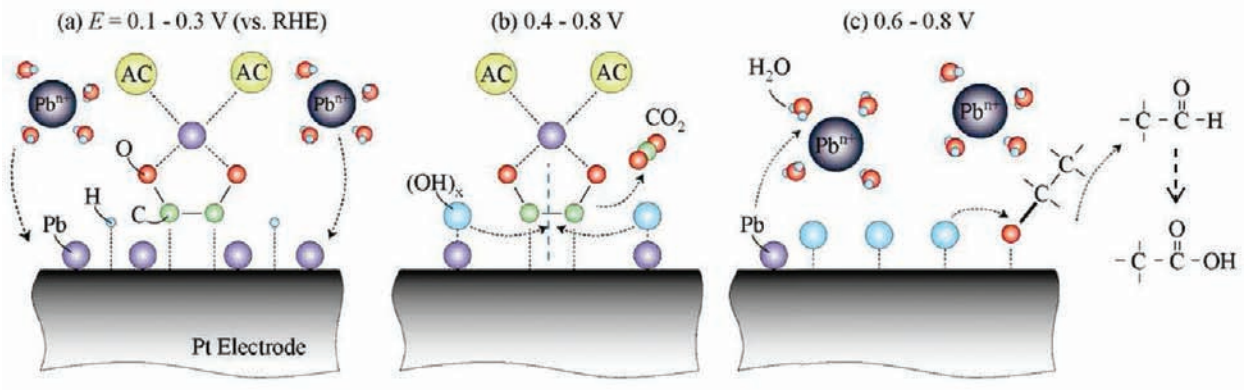


**Figure 10.** Working mechanism of electrooxidation of ethanol on the Pt electrode with the assistance of Pb acetate at different potentials in alkaline media.

bond, giving rise to $CO_2$ in the potential range 0.4−0.8 V. In panel c, at potentials above 0.6 V, more Pb adatoms are expected to leave the surface so that more C2 products are produced. On the other hand, it indicates that it is a self-regeneration system because the Pb adatoms are oxidized and released back into solution to regenerate the Pb(IV) complex.

## 4. CONCLUSIONS

A successful method was developed to significantly enhance the efficiency of electro-oxidation of ethanol in a high pH environment through the addition of Pb(IV) cations. The combination of electrochemical and spectrometric data shows for the first time an effective strategy for combining homogeneous and heterogeneous processes directing both the activity as well as the selectivity of electrocatalytic oxidations of organic molecules, specifically involving cleavage of the C−C bond.

A cathodic shift of 150 mV of the onset potential for ethanol oxidation was observed on a Pt/C electrode in the presence of 1 mM Pb(IV). Chronoamperometric measurements reveal that a steady-state current remains 1 h later (up to 56% of the initial), and is higher than any reported to date. The lead ions were found to play a dual role in the catalysis: $Pb(OH)_2$ is adsorbed on the Pt surface and produces favorably adsorbed OH at lower potentials to oxidize the CO and other carbonyl species, and Pb(II) and/or Pb(IV) ions form a complex with ethanol before it reaches the electrode surface, which appears to be beneficial for the C−C bond breakage either by influencing the orientation of the ethanol as it approaches the surface or even by assisting in the bond breaking directly. The excellent sustained activity shown in the case of ethanol oxidation accompanied with high selectivity to complete oxidation outlines the potential of this strategy for use in electrocatalytic power generating applications.

## ■ ASSOCIATED CONTENT

### Supporting Information

Detailed electrochemical characterizations, *in situ* $\Delta\mu$ XANES analysis, DEMS experiments, and oxygen reduction reaction data in the presence of Pb(IV). This material is available free of charge via the Internet at http://pubs.acs.org.

## ■ AUTHOR INFORMATION

### Corresponding Author

s.mukerjee@neu.edu

### Present Addresses

[⊥]Environmental Energy Technologies Division, Lawrence Berkeley National Laboratory, Berkeley, CA 94720

[∥]X-ray Science Division, Advanced Photon Source, Argonne National Laboratory, Argonne, IL 60439-4858

### Notes

The authors declare no competing financial interest.

## ■ ACKNOWLEDGMENTS

The authors deeply appreciate the financial assistance of the Army Research Office under the Single Investigator grant. Use of the National Synchrotron Light Source, Brookhaven National Laboratory, was supported by the U.S. Department of Energy, Office of Science, Office of Basic Energy Sciences, under Contract No. DE-AC02-98CH10886.

## ■ REFERENCES

(1) Bocarsly, A. B.; Barton, E. E. *Abstracts of Papers*, 237th ACS National Meeting, Salt Lake City, UT, United States, March 22−26, 2009; American Chemical Society: Washington, DC, 2009; INOR-632.

(2) Kim, I.; Han, O. H.; Chae Seen, A.; Paik, Y.; Kwon, S.-H.; Lee, K.-S.; Sung, Y.-E.; Kim, H. *Angew. Chem., Int. Ed.* **2011**, *50*, 2270−2274.

(3) Antolini, E. *J. Power Sources* **2007**, *170*, 1−12.

(4) Corma, A.; Diaz-Cabanas, M. J.; Martinez-Triguero, J.; Rey, F.; Rius, J. *Nature (London, U.K.)* **2002**, *418*, 514−517.

(5) Lai, S. C. S.; Koper, M. T. M. *Faraday Discuss.* **2008**, *140*, 399−416.

(6) Wang, H.; Jusys, Z.; Behm, R. J. *J. Power Sources* **2006**, *154*, 351−359.

(7) Jiang, L.; Colmenares, L.; Jusys, Z.; Sun, G. Q.; Behm, R. J. *Electrochim. Acta* **2007**, *53*, 377−389.

(8) Wang, H.; Zhao, Y.; Jusys, Z.; Behm, R. J. *J. Power Sources* **2006**, *155*, 33−46.

(9) Lai Stanley, C. S.; Koper Marc, T. M. *Phys. Chem. Chem. Phys.* **2009**, *11*, 10446−10456.

(10) Tripkovic, A. V.; Popovic, K. D.; Grgur, B. N.; Blizanac, B.; Ross, P. N.; Markovic, N. M. *Electrochim. Acta* **2002**, *47*, 3707−3714.

(11) Rao, V.; Hariyanto; Cremers, C.; Stimming, U. *Fuel Cells (Weinheim, Ger.)* **2007**, *7*, 417−423.

(12) Mondelli, C.; Grunwaldt, J.-D.; Ferri, D.; Baiker, A. *Phys. Chem. Chem. Phys.* **2010**, *12*, 5307−5316.

(13) Mondelli, C.; Ferri, D.; Grunwaldt, J.-D.; Krumeich, F.; Mangold, S.; Psaro, R.; Baiker, A. *J. Catal.* **2007**, *252*, 77−87.

(14) Grunwaldt, J.-D.; Caravati, M.; Baiker, A. *J. Phys. Chem. B* **2006**, *110*, 25586−25589.

(15) Haan, J. L.; Masel, R. I. *ECS Trans.* **2008**, *16*, 627−638.

(16) Cuesta, A. *ChemPhysChem* **2011**, *12*, 2375−2385.
(17) Xu, C.; Shen, P. K.; Ji, X.; Zeng, R.; Liu, Y. *Electrochem. Commun.* **2005**, *7*, 1305−1308.
(18) Xu, C.; Shen Pei, K. *Chem. Commun. (Cambridge, U.K.)* **2004**, 2238−2239.
(19) Bai, Y.; Wu, J.; Xi, J.; Wang, J.; Zhu, W.; Chen, L.; Qiu, X. *Electrochem. Commun.* **2005**, *7*, 1087−1090.
(20) Kowal, A.; Li, M.; Shao, M.; Sasaki, K.; Vukmirovic, M. B.; Zhang, J.; Marinkovic, N. S.; Liu, P.; Frenkel, A. I.; Adzic, R. R. *Nat. Mater.* **2009**, *8*, 325−330.
(21) Schmiemann, U.; Mueller, U.; Baltruschat, H. *Electrochim. Acta* **1995**, *40*, 99−107.
(22) Gomes Janaina, F.; Busson, B.; Tadjeddine, A. *J. Phys. Chem. B* **2006**, *110*, 5508−5514.
(23) Li, G.; Pickup, P. G. *Electrochim. Acta* **2006**, *52*, 1033−1037.
(24) McBreen, J.; O'Grady, W. E.; Pandya, K. I.; Hoffman, R. W.; Sayers, D. E. *Langmuir* **1987**, *3*, 428−433.
(25) Newville, M. *J. Synchrotron Radiat.* **2001**, *8*, 322−324.
(26) Newville, M.; Livins, P.; Yacoby, Y.; Stern, E. A.; Rehr, J. J. *Phys. Rev. B* **1993**, *47*, 14126.
(27) Scott, F. J.; Mukerjee, S.; Ramaker, D. E. *J. Phys. Chem. C* **2010**, *114*, 442−453.
(28) Teliska, M.; O'Grady, W. E.; Ramaker, D. E. *J. Phys. Chem. B* **2004**, *108*, 2333−2344.
(29) Teliska, M.; O'Grady, W. E.; Ramaker, D. E. *J. Phys. Chem. B* **2005**, *109*, 8076−8084.
(30) van Dorssen, G. E.; Koningsberger, D. C.; Ramaker, D. E. *J. Phys.: Condens. Matter* **2002**, *14*, 13529−13541.
(31) Ankudinov, A. L.; Ravel, B.; Rehr, J. J.; Conradson, S. D. *Phys. Rev. B: Condens. Matter Mater. Phys.* **1998**, *58*, 7565−7576.
(32) Arruda, T. M.; Shyam, B.; Ziegelbauer, J. M.; Mukerjee, S.; Ramaker, D. E. *J. Phys. Chem. C* **2008**, *112*, 18087−18097.
(33) Janin, E.; von Schenck, H.; Gothelid, M.; Karlsson, U. O.; Svensson, M. *Phys. Rev. B: Condens. Matter Mater. Phys.* **2000**, *61*, 13144−13149.
(34) Wang, H.-F.; Liu, Z.-P. *J. Am. Chem. Soc.* **2008**, *130*, 10996−11004.
(35) Souza-Garcia, J.; Herrero, E.; Feliu, J. M. *ChemPhysChem* **2010**, *11*, 1391−1394.
(36) Lai, S. C. S.; Kleijn, S. E. F.; Oeztuerk, F. T. Z.; van Rees Vellinga, V. C.; Koning, J.; Rodriguez, P.; Koper, M. T. M. *Catal. Today* **2010**, *154*, 92−104.
(37) Melke, J.; Schoekel, A.; Dixon, D.; Cremers, C.; Ramaker, D. E.; Roth, C. *J. Phys. Chem. C* **2010**, *114*, 5914−5925.
(38) Pourbaix, M. *Atlas of Electrochemical Equilibria in Aqueous Solutions*; National Association of Corrosion Engineers: Houston, TX, 1974.
(39) Lai, S. C. S.; Kleijn, S. E. F.; Oeztuerk, F. T. Z.; van Rees Vellinga, V. C.; Koning, J.; Rodriguez, P.; Koper, M. T. M. *Catal. Today* **2010**, *154*, 92−104.
(40) Markovic, N. M.; Lucas, C. A.; Rodes, A.; Stamenkovic, V.; Ross, P. N. *Surf. Sci.* **2002**, *499*, L149−L158.
(41) Scott, F. J.; Mukerjee, S.; Ramaker, D. E. *J. Electrochem. Soc.* **2007**, *154*, A396−A406.
(42) Bus, E.; Ramaker, D. E.; van Bokhoven, J. A. *J. Am. Chem. Soc.* **2007**, *129*, 8094−8102.
(43) Strmcnik, D.; Kodama, K.; van der Vliet, D.; Greeley, J.; Stamenkovic, V. R.; Markovic, N. M. *Nat. Chem.* **2009**, *1*, 466−472.
(44) Marken, F.; Leslie, W. M.; Compton, R. G.; Moloney, M. G.; Sanders, E.; Davies, S. G.; Bull, S. D. *J. Electroanal. Chem.* **1997**, *424*, 25−34.